LETTER

Architecture of the mitochondrial calcium uniporter

Kirill Oxenoid[1]*, Ying Dong[2]*, Chan Cao[1,3]*, Tanxing Cui[1]*, Yasemin Sancak[4], Andrew L. Markhard[4], Zenon Grabarek[4], Liangliang Kong[2], Zhijun Liu[2], Bo Ouyang[2], Yao Cong[2], Vamsi K. Mootha[4] & James J. Chou[1,2]

Mitochondria from many eukaryotic clades take up large amounts of calcium (Ca^{2+}) via an inner membrane transporter called the uniporter. Transport by the uniporter is membrane potential dependent and sensitive to ruthenium red or its derivative Ru360 (ref. 1). Electrophysiological studies have shown that the uniporter is an ion channel with remarkably high conductance and selectivity[2]. Ca^{2+} entry into mitochondria is also known to activate the tricarboxylic acid cycle and seems to be crucial for matching the production of ATP in mitochondria with its cytosolic demand[3]. Mitochondrial calcium uniporter (MCU) is the pore-forming and Ca^{2+}-conducting subunit of the uniporter holocomplex, but its primary sequence does not resemble any calcium channel studied to date. Here we report the structure of the pore domain of MCU from *Caenorhabditis elegans*, determined using nuclear magnetic resonance (NMR) and electron microscopy (EM). MCU is a homo-oligomer in which the second transmembrane helix forms a hydrophilic pore across the membrane. The channel assembly represents a new solution of ion channel architecture, and is stabilized by a coiled-coil motif protruding into the mitochondrial matrix. The critical DXXE motif forms the pore entrance, which features two carboxylate rings; based on the ring dimensions and functional mutagenesis, these rings appear to form the selectivity filter. To our knowledge, this is one of the largest membrane protein structures characterized by NMR, and provides a structural blueprint for understanding the function of this channel.

Recently, genomic approaches have revealed the full molecular machinery of the uniporter holocomplex (uniplex)[4–8]. In vertebrates, this complex consists of the transmembrane (TM) domain containing protein MCU, its inactive paralogue MCUb, and an accessory single-pass TM peptide called EMRE. In addition, the complex includes two paralogous, EF-hand Ca^{2+}-binding proteins MICU1 and MICU2 in the intermembrane space. Current models of the uniporter indicate that MCU is the pore-forming subunit, and that MICU1/2 are Ca^{2+}-sensing proteins that gate the activity of the pore based on cytosolic Ca^{2+} concentrations[9]. EMRE is metazoan specific and appears to have two key functions: it maintains the pore in an open conformation, while additionally transducing MICU1/2 Ca^{2+} sensing to the pore[7].

There is consensus now based on several lines of evidence that MCU encodes the pore-forming subunit. First, loss of MCU leads to complete abrogation of uniporter current[4,10]. Second, expression of the MCU orthologue from *Dictyostelium*, an organism that does not have EMRE, is alone sufficient to reconstitute uniporter activity in yeast[11]. Third, MCU has conserved acidic residues in the DXXE sequence motif at the putative entrance of the channel that are essential for Ca^{2+} uptake[4,6]. Fourth, MCU monomers oligomerize into a higher molecular mass assembly[4,11], as would be required of a pore. Fifth, a point mutation in MCU confers resistance to Ru360 while preserving

uniporter current[4,10], providing compelling biochemical evidence that MCU is the probable mechanistic target of Ru360. At present, information on the architecture of this pore protein is lacking. For example, we do not know what its oligomeric state is, which TM helix forms the pore, or what the structural basis of channel regulation is.

To determine the structure of the pore domain of MCU, we used an approach that combines EM and NMR. MCU is predicted to be at least a tetramer[8]. Thus the full-length complex (>160 kDa) is too large for *de novo* structure determination by present solution NMR technology. The protein contains a soluble amino-terminal domain (NTD; $\sim$165 residues) that may be dispensable for channel activity[12] (Fig. 1a). We screened several constructs of MCU with a deleted NTD, and found that the one from *C. elegans* (cMCU-ΔNTD) (Extended Data Fig. 1) could be expressed to high levels in *Escherichia coli*. The protein was extracted using foscholine-14 detergent followed by ion-exchange and size-exclusion chromatography in physiological buffer at pH 6.5 (see Methods). The purified cMCU-ΔNTD in foscholine-14 formed pentamers as suggested by size-exclusion chromatography coupled to multi-angle light scattering (SEC-MALS) and crosslinking (Extended Data Fig. 2), and generated NMR spectra of good chemical shift dispersion and resolution (Fig. 1b and Extended Data Fig. 3). Under the sample condition, cMCU-ΔNTD bound Ru360, and introduction of the Ser238Ala mutation, which was shown previously to confer resistance[4,10], reduced the inhibitor binding (Fig. 1c).

We first performed negative-stain EM reconstruction of the cMCU-ΔNTD oligomers, after diluting NMR sample, using the single particle analysis method (see Methods), with the goal of obtaining a global structural framework to aid subsequent structure determination by NMR. From the 12,860 automatically picked particles, we obtained a reconstructed 3D density map refined to a resolution of $\sim$18 Å (Extended Data Fig. 4). The EM map has a roughly cylindrical shape with five-fold symmetry (Fig. 1d), indicating that cMCU-ΔNTD forms pentamers. Despite the low resolution, the map showed many interesting features. One end of the cylinder has a deep hole, probably corresponding to the TM pore domain, whereas the opposite end is solid, possibly due to the formation of a coiled-coil (CC) complex by the predicted CC helix at the carboxy terminus (Fig. 1a,d). Moreover, each subunit appears to have three levels, and the middle level exhibits an unusual bulge.

The pentameric complex formed by cMCU-ΔNTD has a total molecular mass of $\sim$90,375 Da and thus represents a formidable challenge to NMR spectroscopy. Further challenge came from poor sample stability at temperatures $>$23 °C. Consequently, we recorded NMR data at two different temperatures: 23 °C for collecting the bulk structural restraints and 33 °C for providing information on protein regions that showed weak NMR signals at 23 °C. The general approach we used for structure determination involves: (i) determination of

[1]Department of Biological Chemistry and Molecular Pharmacology, Harvard Medical School, Boston, Massachusetts 02115, USA. [2]State Key Laboratory of Molecular Biology, National Center for Protein Science Shanghai, Shanghai Institute of Biochemistry and Cell Biology, Shanghai Science Research Center, Chinese Academy of Sciences, Shanghai 200031, China. [3]State Key Laboratory of Elemento-Organic Chemistry and College of Chemistry, Nankai University, Tianjin 300071, China. [4]Department of Molecular Biology and Howard Hughes Medical Institute, Massachusetts General Hospital, Boston, Massachusetts 02114, USA.
*These authors contributed equally to this work.
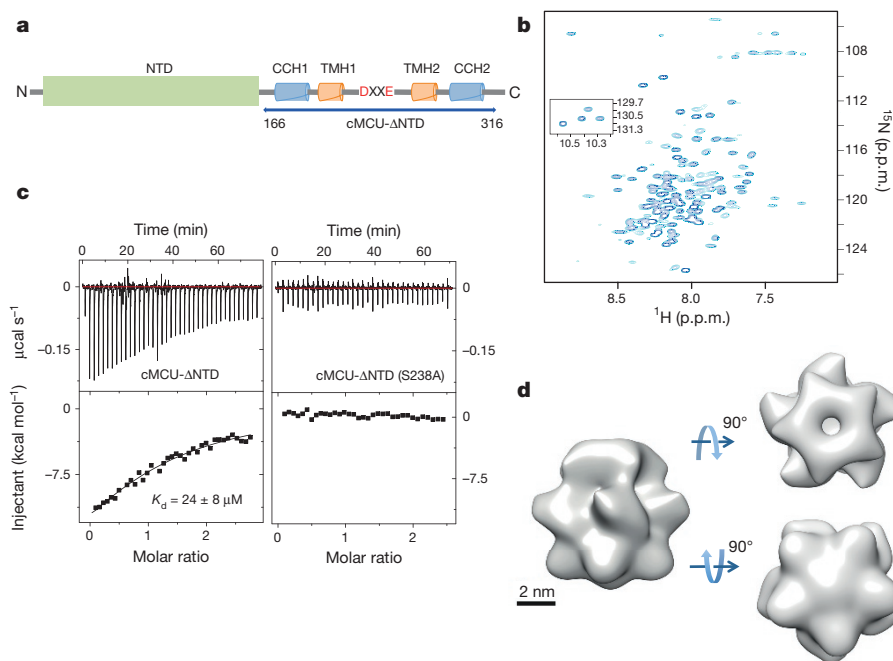
Figure 1 | NMR and EM characterization of cMCU-ΔNTD.
a, Domain organization of MCU (predicted using programs COILS[25] and TMHMM[26]). **b**, ¹H–¹⁵N TROSY heteronuclear single quantum coherence (HSQC) spectrum of (¹⁵N,²H)-labelled cMCU-ΔNTD oligomer reconstituted in foscholine-14, recorded at 900 MHz and 23 °C. The peaks in the inset correspond to tryptophan side-chain amines. **c**, Isothermal titration calorimetry (ITC) analysis of Ru360 binding to cMCU-ΔNTD (left) and the Ser238Ala mutant (right) under the NMR sample condition.

The top and bottom graphs show the raw data (μcal s⁻¹ versus time) and normalized integration data (kcal mol⁻¹ of injectant versus molar ratio; molar ratio = Ru360:cMCU-ΔNTD pentamer), respectively. Data fitting yields dissociation constant (K_d) = 24 ± 8 μM. **d**, Negative stain EM reconstruction of the cMCU-ΔNTD oligomers using a protein sample prepared in the same way as NMR samples. Views of the final 3D volumes of cMCU-ΔNTD oligomer filtered at 18 Å.

local structures of the monomers, and (ii) assembly of the oligomer with intermonomer distance restraints[13–15]. The secondary structures of the monomers in the oligomeric complex were determined mainly using local distance restraints derived from nuclear Overhauser enhancements (NOEs). We then used a mixed sample with differentially labelled subunits to measure exclusively NOEs between the ¹⁵N-attached protons of one subunit and non-exchangeable protons of the neighbouring subunits. This experiment provided key intermonomer NOEs defining the CC, the TM pore, and the ion-selectivity domains (Extended Data Fig. 5). The initial structural solution then allowed iterative assignment of additional intermonomer and long-range NOEs using standard NOE experiments. The structure was determined using 2,070 local and 150 long-range intramonomer distance restraints and 220 intermonomer restraints (Extended Data Fig. 6a and Extended Data Table 1).

The NMR structure of cMCU-ΔNTD shows a well-packed pentamer with an overall cylindrical shape similar to the EM map (Extended Data Fig. 6b–e). The EM structure is slightly shorter and wider than the NMR structure, which could have been caused by specimen flattening, a phenomenon commonly observed in negative stain EM[16]. Both have a star-like appearance when viewed from top or bottom, and feature five bulges in the middle of the assembly that curve in the same direction (Figs 2a and 1d). The more detailed NMR structure revealed the architecture of the channel assembly. The inner core of the pentamer is formed with the second TM helix (TMH2; 244–260) and the coiled-coil helix (CCH; residues 293–316) (Fig. 2b, c). While the TMH2s pack into a five-helix bundle having a largely polar pore across the membrane, the CCH outside the membrane forms a CC pentamer with a hydrophobic core, which may contribute to stabilizing the TM pore structure. As an independent validation of the pentameric assembly of the CCH, we showed by chemical crosslinking that a peptide containing the predicted CC domain (residues 289–316) in water forms a pentamer in agreement with the oligomeric state of cMCU-ΔNTD (Methods; Extended Data Fig. 7). The two core domains are

structurally supported by peripheral helices: the TM pore domain is wrapped by the first TM helix (TMH1; residues 215–234) through contacts between TMH1 and TMH2, and the extramembrane CC domain is wrapped by the first helix of cMCU-ΔNTD (H1; residues 180–193) (Fig. 2b, c). The two core domains are not continuous as TMH2 ends at Tyr260, which is immediately followed by the inner juxtamembrane helix (IJMH; residues 262–271) that orients at a wide angle relative to TMH2. The IJMH turns into an unstructured loop (L2; residues 272–292) before the beginning of the CCH. NMR peaks for many of the residues in L2 were not observed, possibly owing to solvent exchange and conformational heterogeneity. The two core domains appear to be held together on the periphery by the outer juxtamembrane helix (OJMH; residues 195–213), which contains a kink around Glu204 and interacts with the IJMH. Despite the apparent structure, NMR signals for IJMH and OJMH are mostly weak due to exchange broadening, suggesting the membrane proximal region of cMCU-ΔNTD is intrinsically unstable. In addition to L2, another unstructured region is the loop preceding H1 (L1; residues 166–179); it is unstructured due to the absence of NTD as residues 166–171 in the corresponding NTD of human MCU form a short helix[12].

The structure suggests a Ca²⁺ flow pathway through the MCU pore. The critical DXXE motif connecting TMH1 and TMH2 forms a pentameric barrel that appears to be the mouth of the pore (Fig. 3a). Inside the barrel, both acidic residues are in position to form two carboxylate rings. The Asp240 ring is solvent exposed, and the Glu243 ring is located deeper, guarding the entrance of the TMH2 pore commencing at Pro244. The precise ring sizes cannot be measured in our structure because the Asp240 and Glu243 side chains could not be precisely defined using the available NOE restraints (Fig. 3b), but the diameter of the ring defined by Cβ is 7 Å and 11 Å for Asp240 and Glu243, respectively. These values are smaller on average than those of the asparagine ring in the CorA Mg²⁺ channel (11 Å)[17–20] or the glutamate ring in the Orai Ca²⁺ channel (12 Å)[21], suggesting that Ca²⁺ should be partially dehydrated by the Asp240 and Glu243 rings.
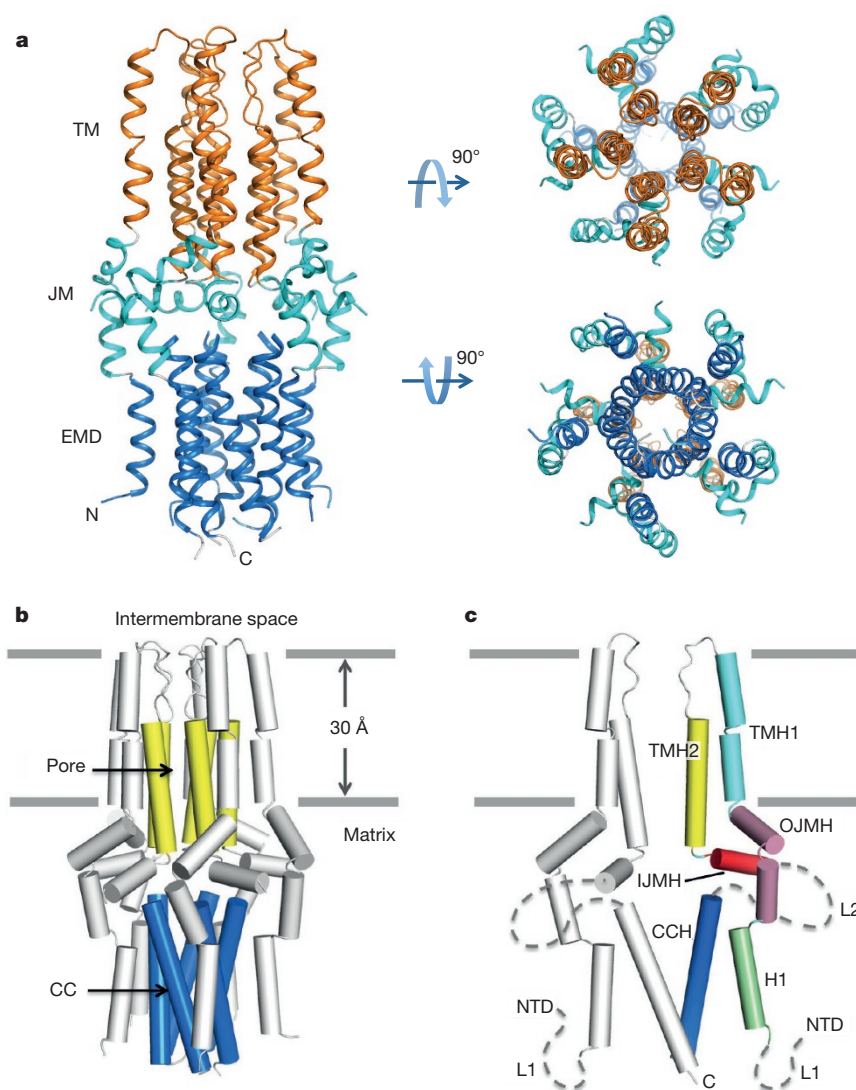
Figure 2 | Structure of the cMCU-ΔNTD pentamer. a, Ribbon representation of the cMCU-ΔNTD structure displaying three distinct layers that correspond to the transmembrane (TM; orange), juxtamembrane (JM; cyan), and extramembrane domain (EMD; blue) regions, respectively. **b**, Cartoon representation of the cMCU-ΔNTD pentamer showing the formation of the uniporter core, which consists of the TM pore formed by TMH2 (yellow) and the coiled-coil pentamer

formed by CCH (marine). The structure is placed in the presumed membrane such that the peripheral hydrophobic residues in the TM domain are lipid facing. **c**, Cartoon representation of two subunits of the cMCU-ΔNTD pentamer showing the folding of individual subunits. The helical segments are defined in the text. The dashed lines labelled as L1 and L2 correspond to the unstructured regions of the protein.

Passing the acidic rings, Ca^{2+} can readily move through the TM pore, which is hydrophilic and lined mostly with threonines (Fig. 3c and Extended Data Fig. 8). The TM pore ends with Tyr260. Upon exiting the TM pore from the C-terminal end, Ca^{2+} will be in a very hydrophilic chamber enclosed by IJMH and OJMH on the side and the CC domain on the bottom (Fig. 2b, c). Ca^{2+} cannot exit through the CC domain because this domain has a solid hydrophobic core. Surface plot also shows that interaction between IJMH and OJMH seals the side of the chamber leaving no visible holes for ions to exit laterally (Fig. 3d). Thus, the structure represents the closed conformation of the channel, which is consistent with the fact that metazoan MCU in the absence of EMRE does not transport Ca^{2+} (refs 7, 11). We speculate that conformational rearrangements induced by EMRE binding are needed to allow Ca^{2+} to exit. By nature of being unstable, the IJMH, OJMH and L2 segments of each MCU monomer are the likely regions to undergo conformational changes that would create lateral exit paths near the membrane, each activated by its own EMRE peptide.

The structure of cMCU-ΔNTD provides a framework for better understanding human MCU (HsMCU), especially because HsMCU

and cMCU are orthologous, with greater than 40% sequence identity, sharing the same protein domain organization[22]. We previously reported the use of HEK-293T cells in which we knocked out HsMCU[7]. Such cells do not exhibit mitochondrial Ca^{2+} uptake, and represent an excellent system into which we can introduce mutant alleles to evaluate their effect on mitochondrial Ca^{2+} uptake. We created the NTD deletion in HsMCU (HsMCU-ΔNTD), corresponding to deletion in cMCU-ΔNTD, and found that the mutant is able to complement the need for HsMCU, demonstrating that the NTD in the human protein is dispensable for calcium uptake activity (Extended Data Fig. 9). We then created a cysteine-free mutant of HsMCU (HsMCU^{CF}) akin to cMCU-ΔNTD, and found that it could rescue Ca^{2+} transport in human cells lacking MCU (Fig. 4a). We next proceeded to introduce mutations into HsMCU^{CF} to validate our NMR structure of cMCU-ΔNTD. Glu257 (Glu236 in cMCU) is highly conserved across eukaryotic MCU orthologues, but it is not conserved in MCUb, a non-conducting human paralogue of MCU. It was proposed that this residue is key to Ca^{2+} conductance[4,8] because transient expression of Glu257Ala mutant on a partial MCU knockdown background failed
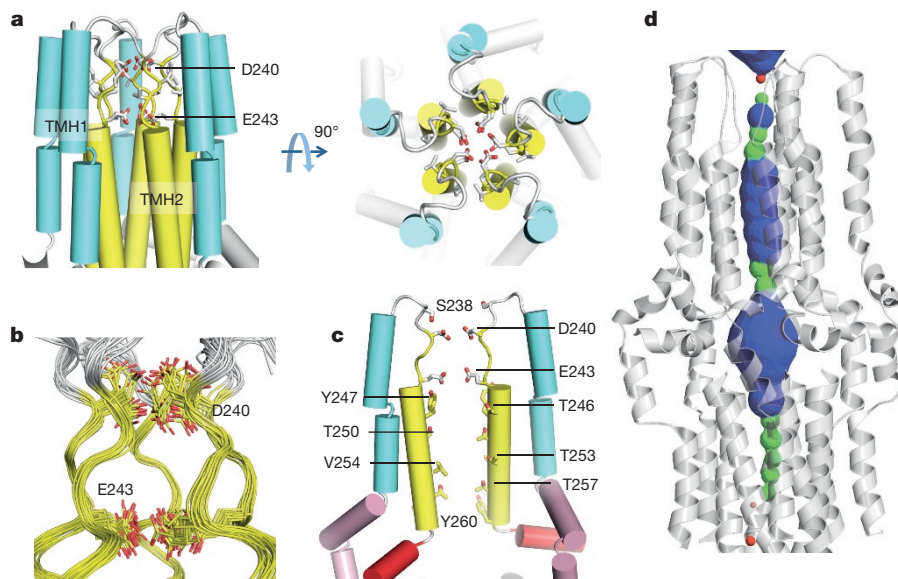
Figure 3 | Architecture of the pore and ion selectivity filter. a, Cartoon representation of the TM domain displaying the mini barrel at the mouth of the TM pore that contains the DXXE Ca^{2+} selectivity elements. **b**, Enlarged view of the DXXE-containing region for showing side-chain conformational diversity of Asp240 and Glu243. **c**, TM domains of subunits 1 and 3 for showing the pore-lining residues. **d**, The pore surface calculated using the program HOLE[27]. The region of the channel colored in green is only wide enough to allow passage of one water molecule, whereas the blue portion can accommodate two or more water molecules. The red region is too narrow to allow any water to pass through.

to rescue calcium transport fully. However, our structure (Fig. 3a, c) places this residue outside the entrance of the pore, and predicts it to be dispensable for Ca^{2+} uptake. Indeed, consistent with this prediction, we find that when Glu257Ala or Glu257Ser mutants are stably expressed at levels comparable to that of wild-type protein on a clean MCU knockout background, they conduct Ca^{2+} (Fig. 4b). In contrast to Glu257, substitutions of Asp or Glu within the DXXE motif with Ala disrupted mitochondrial Ca^{2+} uptake[4]. Our structure shows that the side chains of these residues provide two carboxylate rings that might be involved in Ca^{2+} permeation and/or selectivity. Given how critical these two residues appear to be in the structure, we made very conservative mutations, namely Asp261Glu and Glu264Asp (Asp240 and Glu243 in cMCU). While Asp261Glu is partially functional, we note that Glu264Asp has completely lost its ability to conduct Ca^{2+} despite

expressing properly (Fig. 4c), underscoring the critical importance of this residue for permeation.

We next considered the mechanism of action of the drug Ru360, a well-known inhibitor of the uniporter. Ru360 inhibits the human uniporter with nanomolar potency in isolated mitochondria or in permeabilized cells. We previously identified Ser259 (Ser238 in cMCU) as being potentially important for the mechanism of action of Ru360, since the Ser259Ala mutant permits Ca^{2+} conductance but confers nearly complete resistance against Ru360 (refs 4, 10). In our structure of cMCU-ΔNTD, this serine residue lies at the apex of the pore, before the mini-barrel, raising the hypothesis that Ru360 operates by simply obstructing the pore. If this hypothesis is correct, then the introduction of bulky residues into this position ought to occlude the pore. In fact, Ser259Arg is well expressed and does not permit any Ca^{2+} to
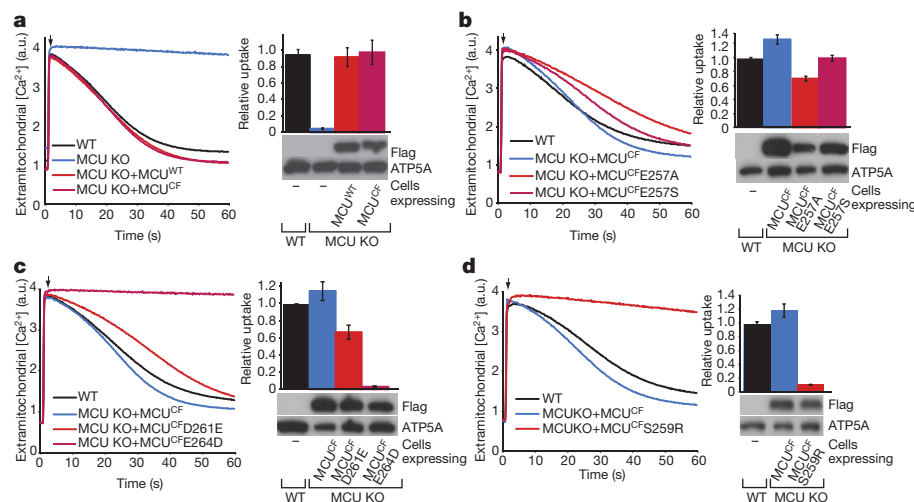
Figure 4 | Functional mutagenesis of HsMCU inspired by the cMCU-ΔNTD structure. a, Cysteine-free MCU (MCU^{CF}) rescues mitochondrial calcium uptake to the same extent as wild-type MCU (MCU^{WT}) in MCU knockout (KO) cells. **b**, Mutation of MCU Glu257 to Ala or Ser does not impair its function. **c**, Mutation of Asp261 to Glu permits ion permeation through MCU whereas Glu264 to Asp impairs function. **d**, Mutation of Ser259 to Arg impairs MCU function. **a–d**, Representative traces of Ca^{2+} uptake in digitonin-permeabilized cells after addition of 50 μM $CaCl_2$ are shown on left. The bar graph shows the rate of Ca^{2+} uptake relative to wild-type HEK-293T cells (mean ± s.d., $n = 4$). Cell lysates were analysed by immunoblotting using anti-Flag antibody to detect expression of MCU protein. ATP5A was used as loading control.

enter, probably mimicking the effect of Ru360 (Fig. 4d). Collectively, these experiments demonstrate the value of our structure for understanding the function of human MCU.

The cMCU-ΔNTD structure represents a new solution of ion channel architecture. The bacterial and mitochondrial Mg^{2+} channel, CorA/MRS2, also forms a pentamer and has a similar domain organization based on primary and secondary structures, but it has very different tertiary and quaternary fold[19,20]. The TM domains of both CorA and MCU are composed of ten helices (two from each subunit) arranged in two concentric layers. Whereas the CorA pore is formed by TMH1, the MCU pore is formed by TMH2. The selectivity filter in MCU appears to be composed of two carboxylate rings: the solvent-accessible aspartate and the internal glutamate rings (Fig. 3a, b). In CorA, the solvent-accessible ring is made of five asparagines, and the slightly larger internal ring of backbone carbonyls of glycine residues[17]. By contrast, the Ca^{2+} release activated Ca^{2+} channel Orai has only one ring of six glutamate side chains in the filter region[21]. Another major difference between CorA and Orai on the one hand and MCU on the other is that after the selectivity filter, the pore in both CorA and Orai becomes hydrophobic for several helical turns. In MCU, however, the pore remains hydrophilic suggesting an explanation for fast ion conduction by this channel. Finally, in Orai and CorA, the ion pathway continues far beyond the membrane bilayer, but in MCU the pore ends after traversing the bilayer, with ions likely exiting laterally near the membrane. In this respect the architecture of cMCU-ΔNTD is reminiscent of some channel proteins that belong to the diverse family of pentameric ligand gated ion channels (pLGIC), which includes serotonin 5-HT_3 and nicotinic acetylcholine receptors[23,24].

In conclusion, the combined use of NMR and EM enabled the characterization of the overall architecture of the MCU, which is also one of the largest membrane protein complexes studied by NMR. The structure represents a new pore architecture for conducting Ca^{2+} as its ion-selectivity filter, ion-conducting pore, and the arrangement of the extramembrane domains are all different from the known Ca^{2+} channel structures. Although the reported structure does not show Ca^{2+} exit, which is consistent with being non-conducting in the absence of EMRE, the overall architecture suggests lateral Ca^{2+} exit near the middle of the channel complex. Several outstanding questions remain. The structure shows the selectivity filter and the pore, yet the detailed mechanism of Ca^{2+} binding, transport, and exit is unknown, including the function of the L2 loop that could block the exit, but is unstructured in our model. Although we have provided compelling evidence that cMCU forms a pentamer *in vitro*, the oligomeric state *in vivo* remains to be confirmed. Finally, MCU interactions with its TM partner EMRE and its regulators MICU1/2 are important subjects of future investigation.

Online Content Methods, along with any additional Extended Data display items and Source Data, are available in the online version of the paper; references unique to these sections appear only in the online paper.

1. Gunter, T. E. & Pfeiffer, D. R. Mechanisms by which mitochondria transport calcium. *Am. J. Physiol.* **258**, C755–C786 (1990).
2. Kirichok, Y., Krapivinsky, G. & Clapham, D. E. The mitochondrial calcium uniporter is a highly selective ion channel. *Nature* **427**, 360–364 (2004).
3. Denton, R. M. & McCormack, J. G. The role of calcium in the regulation of mitochondrial metabolism. *Biochem. Soc. Trans.* **8**, 266–268 (1980).
4. Baughman, J. M. *et al.* Integrative genomics identifies MCU as an essential component of the mitochondrial calcium uniporter. *Nature* **476**, 341–345 (2011).
5. Perocchi, F. *et al.* MICU1 encodes a mitochondrial EF hand protein required for Ca^{2+} uptake. *Nature* **467**, 291–296 (2010).
6. De Stefani, D., Raffaello, A., Teardo, E., Szabo, I. & Rizzuto, R. A forty-kilodalton protein of the inner membrane is the mitochondrial calcium uniporter. *Nature* **476**, 336–340 (2011).
7. Sancak, Y. *et al.* EMRE is an essential component of the mitochondrial calcium uniporter complex. *Science* **342**, 1379–1382 (2013).
8. Raffaello, A. *et al.* The mitochondrial calcium uniporter is a multimer that can include a dominant-negative pore-forming subunit. *EMBO J.* **32**, 2362–2376 (2013).
9. Kamer, K. J. & Mootha, V. K. The molecular era of the mitochondrial calcium uniporter. *Nature Rev. Mol. Cell Biol.* **16**, 545–553 (2015).
10. Chaudhuri, D., Sancak, Y., Mootha, V. K. & Clapham, D. E. MCU encodes the pore conducting mitochondrial calcium currents. *eLife* **2**, e00704 (2013).
11. Kovács-Bogdán, E. *et al.* Reconstitution of the mitochondrial calcium uniporter in yeast. *Proc. Natl Acad. Sci. USA* **111**, 8985–8990 (2014).
12. Lee, Y. *et al.* Structure and function of the N-terminal domain of the human mitochondrial calcium uniporter. *EMBO Rep.* (2015).
13. Van Horn, W. D. *et al.* Solution nuclear magnetic resonance structure of membrane-integral diacylglycerol kinase. *Science* **324**, 1726–1729 (2009).
14. Schnell, J. R. & Chou, J. J. Structure and mechanism of the M2 proton channel of influenza A virus. *Nature* **451**, 591–595 (2008).
15. OuYang, B. *et al.* Unusual architecture of the p7 channel from hepatitis C virus. *Nature* **498**, 521–525 (2013).
16. Cheng, Y. *et al.* Single particle reconstructions of the transferrin-transferrin receptor complex obtained with different specimen preparation techniques. *J. Mol. Biol.* **355**, 1048–1065 (2006).
17. Guskov, A. *et al.* Structural insights into the mechanisms of Mg^{2+} uptake, transport, and gating by CorA. *Proc. Natl Acad. Sci. USA* **109**, 18459–18464 (2012).
18. Pfoh, R. *et al.* Structural asymmetry in the magnesium channel CorA points to sequential allosteric regulation. *Proc. Natl Acad. Sci. USA* **109**, 18809–18814 (2012).
19. Eshaghi, S. *et al.* Crystal structure of a divalent metal ion transporter CorA at 2.9 angstrom resolution. *Science* **313**, 354–357 (2006).
20. Lunin, V. V. *et al.* Crystal structure of the CorA Mg^{2+} transporter. *Nature* **440**, 833–837 (2006).
21. Hou, X., Pedi, L., Diver, M. M. & Long, S. B. Crystal structure of the calcium release-activated calcium channel Orai. *Science* **338**, 1308–1313 (2012).
22. Bick, A. G., Calvo, S. E. & Mootha, V. K. Evolutionary diversity of the mitochondrial calcium uniporter. *Science* **336**, 886 (2012).
23. Hassaine, G. *et al.* X-ray structure of the mouse serotonin 5-HT_3 receptor. *Nature* **512**, 276–281 (2014).
24. Unwin, N. Refined structure of the nicotinic acetylcholine receptor at 4 Å resolution. *J. Mol. Biol.* **346**, 967–989 (2005).
25. Lupas, A., Van Dyke, M. & Stock, J. Predicting coiled coils from protein sequences. *Science* **252**, 1162–1164 (1991).
26. Sonnhammer, E. L., von Heijne, G. & Krogh, A. A hidden Markov model for predicting transmembrane helices in protein sequences. *Proc. Int. Conf. Intell. Syst. Mol. Biol.* **6**, 175–182 (1998).
27. Smart, O. S., Neduvelil, J. G., Wang, X., Wallace, B. A. & Sansom, M. S. HOLE: a program for the analysis of the pore dimensions of ion channel structural models. *J. Mol. Graph.* **14**, 354–360 (1996).

METHODS

No statistical methods were used to predetermine sample size. The experiments were not randomized and the investigators were not blinded to allocation during experiments and outcome assessment.

Protein sample preparation. *E. coli*-codon optimized DNA encoding residues 167–316 of the *C. elegans* MCU (cMCU-ΔNTD) with C-terminal 6×His tag was synthesized (GenScript) and cloned into the pET21a vector (Extended Data Fig. 1). BL21(DE3) cells were transformed with the vector for expression. The cells were grown in either LB broth or isotopically labelled M9 minimal media at 37 °C until absorbance at 600 nm ($A_{600\,nm}$) reached 0.6–0.7. After induction with 0.2 mM iso-propyl-β-D-thiogalactopyranoside (IPTG), protein was expressed for 20 h at 18 °C. Cells were collected by centrifugation and resuspended and lysed by sonication in buffer A (20 mM HEPES, pH 7.4, 150 mM NaCl, 10 μg ml^{-1} lysozyme, 10 μg ml^{-1} DNase, 1 mM PMSF and 2 mM EDTA). After lysis, the inclusion bodies and membranes were collected by centrifugation at 39,000*g* for 1 h and resuspended in buffer B (20 mM HEPES, pH 7.4, 150 mM NaCl, 40 mM foscholine-14 and 2 mM EDTA), followed by stirring at 4 °C overnight. Insoluble aggregates were removed by centrifugation at 39,000*g* for 40 min. The supernatant was then subjected to Ni-NTA purification in buffer B with foscholine-14 concentration adjusted to 0.48 mM (4× detergent CMC). The protein was eluted using 400 mM imidazole in the same buffer and dialysed against buffer C (25 mM CHES, pH 9.2, 50 mM NaCl and 2 mM EDTA) to remove imidazole. After dialysis, the sample was subjected to ion-exchange purification using the HiTrap Q HP (1 ml) column (GE Healthcare) in buffer C with added 0.48 mM foscholine-14. The protein was eluted using a NaCl gradient (0.05–1.00 M in 20 ml). Finally, the protein was further separated by size exclusion using the Superdex 200 10/300 GL column (GE Healthcare) in buffer D (20 mM MES, pH 6.4, 75 mM NaCl, 0.48 mM foscholine-14, 0.3 mM NaN$_3$, and 2 mM EDTA). The elution peak fractions were analysed by SDS–PAGE (Extended Data Fig. 2) and pooled and concentrated to achieve 0.8 mM cMCU-ΔNTD (monomer) for NMR measurements. The final NMR sample buffer contains 20 mM MES, pH 6.4, 75 mM NaCl, ~27 mM foscholine-14, 0.3 mM NaN$_3$, 2 mM EDTA and 5% D$_2$O. Typical final yields of cMCU-ΔNTD were 2–3 mg of protein from 1 l of cell culture.

SEC-MALS analysis of the cMCU-ΔNTD molecular mass. The instrument setup used for the SEC-MALS experiment consisted of an Agilent 1260 Infinity Isocratic Liquid Chromatography System connected in series with a Wyatt Dawn Heleos II Multi-Angle Light Scattering (MALS) detector (Wyatt Technology) and a Wyatt Optilab T-rEX Refractive Index Detector (Wyatt Technology). Analytical size-exclusion chromatography was performed at room temperature using Superdex 200 10/300 GL column (GE Healthcare) equilibrated with a mobile phase containing 20 mM MES, pH 6.4, 75 mM NaCl, 0.48 mM foscholine-14, 0.3 mM NaN$_3$ and 2 mM EDTA. 100 μl purified cMCU-ΔNTD sample at 4.0 mg ml^{-1} was injected into the column and eluted at a flow rate of 0.4 ml min^{-1}. The column effluent was monitored in-line with three detectors that simultaneously monitored UV absorption, light scattering and refractive index. The data from the three detectors were imported by the ASTRA software package, and the three-detector method[28] was used to determine the molecular mass.

Characterization of the cMCU-ΔNTD oligomeric state by crosslinking. The oligomeric state of cMCU-ΔNTD in the NMR sample was examined by chemical crosslinking using DTSSP (3,3′-dithiobis(sulfosuccinimidyl propionate) (Thermo Scientific)). The cMCU-ΔNTD sample was first dialysed overnight against the crosslinking reaction buffer (25 mM sodium phosphate, pH 7.5, and 50 mM NaCl). A stock solution of 50 mM DTSSP in the reaction buffer was prepared for addition to the protein solution. Five samples each containing 0.1 mM cMCU-ΔNTD in 30 μl reaction buffer were mixed with 0, 5, 7, 10 and 15 mM DTSSP, respectively, at room temperature. After 1 h, the reactions were quenched by adding 2 μl of the stop solution (1 M Tris, pH 7.5). The reaction mixtures were analysed using SDS–PAGE, and visualized using silver stain.

ITC analysis of Ru360 binding. ITC was used to investigate whether cMCU-ΔNTD can interact with the known inhibitor Ru360 under the NMR sample condition. The protein samples used for ITC consisted of 20 mM MES pH 6.4, 75 mM sodium chloride, 4 mM foscholine-14 and 76 μM cMCU-ΔNTD (monomer). The inhibitor solution contained 200 μM Ru360 in 20 mM MES, pH 6.4, 75 mM sodium chloride and 4 mM foscholine-14. The titration protocol involved injecting 0.5 μl inhibitor solution to 202 μl protein solution for the first point and 1 μl for each of the following 34 points (Extended Data Fig. 1c). Experiments were performed at 25 °C using Microcal ITC200 (GE Healthcare). The same ITC experiment was also performed for the cMCU-ΔNTD mutant with the S238A mutation.

Negative stain EM analysis. For EM analysis, the protein sample obtained from the size-exclusion chromatography above was subjected to two more rounds of size exclusion to achieve even higher homogeneity. The middle 20% of the elution peak was collected and subjected to another round of size-exclusion purification

under the same condition. The middle 20% of the elution from the second size exclusion run was collected and subjected to a third round of size exclusion. Finally, the middle 20% of the third elution was collected as the final sample for EM study.

To prepare sample for collecting negative stain EM images, 5 μl of the cMCU-ΔNTD sample from the third size exclusion run (10 μg ml^{-1} protein in 20 mM MES, pH 6.5, 75 mM NaCl, 0.48 mM foscholine-14, 1× protease inhibitor cocktail (Thermo) and 0.1 mM NaN$_3$) was applied to a glow-discharged 400 mesh continuous carbon grid (Beijing Zhongjingkeyi Technology). The sample was then negatively stained with 0.75% (wt/vol) uranyl formate solution, and spontaneously dried at room temperature. The data were recorded on a Tecnai G2 Spirit BioTWIN transmission electron microscope (FEI) operated at 120 kV and equipped with an Eagle 4 K × 4 K CCD camera. We recorded 514 images at 110,000 microscope magnification with a pixel size of 1.05 Å per pixel. The defocus ranged from 1.0 to 1.5 μm. For initial model building, Random Conical Tilt (RCT) image pairs were manually taken at tilt angles of 45° and 0°, respectively.

We boxed out 12,860 particles by using the e2boxer.py program in EMAN2.1 (ref. 29) (Extended Data Fig. 4a). Contrast transfer function parameters were determined for particles boxed out from each CCD image using EMAN1.9 (ref. 30) procedure ctfit, followed by phase flipping using the applyctf program. The data were then low-pass filtered to 10 Å to enhance the image contrast for three-dimensional (3D) reconstruction[31]. Reference-free 2D analysis used the EMAN1.9 program refine2d.py, which revealed the existence of five-fold symmetry in the cMCU-ΔNTD sample (Extended Data Fig. 4b). The initial model was generated from RCT data using e2rct.py program in EMAN2.1. This model was further refined with the 12,860 untilted particles by using the refine program and calling the FRM2D image alignment kernel[32,33] in EMAN1.9. Initially, no symmetry was imposed in the 3D reconstruction process (Extended Data Fig. 4c), and subsequently the five-fold symmetry revealed by reference-free 2D analysis was imposed in the 3D reconstruction process. The final resolution was estimated at 18 Å by the 0.5 FSC criteria using the eotest program in EMAN1.9 (Extended Data Fig. 4d).

Assignment of NMR resonances. All NMR experiments were conducted at either 23 °C or 33 °C on Bruker spectrometers equipped with cryogenic probes. NMR spectra were processed using NMRPipe[34] and analysed using ccpNMR[35] and Xeasy[36]. Sequence-specific assignment of backbone $^1H^N$, ^{15}N, $^{13}C^a$, $^{13}C^b$ and $^{13}C'$ chemical shifts was achieved using the TROSY versions of standard triple resonance experiments including HNCA, HN(CO)CA, HNCACB, HN(CA)CO and HNCO[37,38]. In addition, a 3D HSQC-NOESY-TROSY experiment with ^{15}N, ^{15}N and $^1H^N$ evolution in the t_1, t_2 and t_3 dimensions, respectively, was recorded with an NOE mixing time (t_{NOE}) of 200 ms. These experiments were performed using multiple (^{15}N, ^{13}C, ^2H)-labelled protein samples on a 600 MHz spectrometer at 33 °C. Multiple samples were used due to the poor stability of the protein at temperature >23 °C, that is, the sample began to show precipitation after ~7 days at 33 °C. Despite the problem, the higher temperature was used to obtain more favourable T$_2$ for triple resonance experiments. By combining the triple resonance data with the use of NOESY, we were able to confidently assign 91% of non-proline residues, although only 77% could be assigned if using only the triple resonance spectra. Protein aliphatic and aromatic resonances were assigned using a combination of 2D ^{13}C-edited HSQC, 3D ^{15}N-edited NOESY-TROSY ($t_{NOE} = 100$ ms) and ^{13}C-edited NOESY-HSQC ($t_{NOE} = 150$ ms) recorded on a 900 MHz spectrometer at both 23 °C and 33 °C. These experiments were performed using multiple (^{15}N, ^{13}C)-labelled protein samples in which foscholine-14 was deuterated (Anatrace). The data sets recorded at two different temperatures provided complementary information. On average, the spectra at 23 °C show stronger peaks for the extramembrane regions but very weak peaks for the TM pore domain, especially the selectivity segment, possibly due to higher rigidity of the TM domain. At 33 °C, however, the TM resonances that were too weak to analyse in the 23 °C spectra became sufficiently intense.

Assignment of NOEs. Short-range NOEs used for defining local and secondary structures were assigned using the ^{15}N-edited NOESY-TROSY and ^{13}C-edited NOESY-HSQC recorded at two different temperatures as described above. Intermonomer NOEs between the backbone amide protons of a monomer and the non-exchangeable aliphatic or aromatic protons of its neighbouring monomers were assigned using a sample that was reconstituted with approximately 1:1 mixture of (^{15}N, ^2H)-labelled cMCU-ΔNTD and (15% ^{13}C)-labelled cMCU-ΔNTD. The non-deuterated subunit was (15% ^{13}C)-labelled for recording the ^1H–^{13}C HSQC spectrum (optimized for methyl groups) as internal aliphatic proton chemical shift reference while providing stereospecific assignment of leucine and valine methyl groups[39]. Mixing was done at the cell level before cell lysis, that is, the amounts of differently labelled cells were adjusted based on the protein expression level to ensure approximately 1:1 ratio of (^{15}N, ^2H)- and (15% ^{13}C)-labelled cMCU-ΔNTD. In this sample, foscholine-14 was also deuterated. Recording a ^{15}N-edited

NOESY-TROSY using this sample allowed exclusive detection of NOE cross peaks between the ^{15}N-attached protons of one monomer and aliphatic protons of adjacent monomers. The 3D ^{15}N-edited NOESY-TROSY (τ_{NOE}] = 300 ms) was recorded using this type of sample at both 23 °C and 33 °C. The intermonomer NOEs between the neighbouring CCHs and TMH2s (see main text) effectively defined the core of the cMCU-ΔNTD complex. The initial structural solution of the core assembly then allowed us to assign iteratively additional intra- and intermonomer long-range NOEs between the aliphatic and aromatic protons in ^{15}N-edited NOESY-TROSY and ^{13}C-edited NOESY-HSQC recorded at both 23 °C and 33 °C. These long-range NOEs subsequently defined packing of TMH1 against TMH2, packing of H1 against CCH, as well as interaction between IJMH and OJMH.

Structure calculation. Structures were calculated using the program XPLOR-NIH[40]. The local and secondary structures of the monomer were first defined using short-range NOE restraints and backbone dihedral restraints derived from chemical shifts (using TALOS+[41]). A total of 10 monomer structures were calculated using a standard simulated annealing protocol. Five copies of the lowest-energy monomer structure were used to construct an initial model of the pentamer using the intermonomer NOE restraints assigned for the pore-forming TMH2 and CCH helices. For each intermonomer restraint between two adjacent monomers, five identical distance restraints were assigned respectively to all pairs of neighbouring monomers to satisfy the condition of C5 rotational symmetry (as indicated by the EM reconstruction). The assembled pentamer was used as a starting model to guide assignment of more long-range NOEs in the ^{15}N-edited and ^{13}C-edited NOE spectra recorded at 23 °C and 33 °C. This process was repeated iteratively until the calculated models converged to backbone r.m.s.d. of <1 Å (not including the disordered regions). In each of the iterations, the starting model was refined against dihedral restraints and local and long-range intra- and intermonomer NOE restraints using a simulated annealing protocol in which the bath was cooled from 1,000 to 100 K. The NOE restraints were enforced by flat-well harmonic potentials, with the force constant ramped from 25 to 50 kcal mol^{-1} Å^{-2} during annealing. For the defined helical regions, backbone dihedral angle restraints ($\Phi = -60°$, $\Psi = -40°$) were applied, all with a flat-well ($\pm10°$) harmonic potential with force constant ramped from 15 to 30 kcal mol^{-1} rad^{-2}. In the final round of refinement, a total of 150 structures were calculated and 15 low-energy structures were selected as the structural ensemble. Ramachandran plot statistics for the structure ensemble, calculated using PROCHECK[42], are as follows: most favoured (86.3%), additionally allowed (11.0%), generously allowed (1.8%) and disallowed (1.0%). Restraint and refinement statistics are shown in Extended Data Table 1.

Characterization of the oligomeric state of the CCH peptide by crosslinking. To examine whether the C-terminal CCH domain is able to oligomerize by itself in water, we investigated the oligomeric state of a CCH-containing peptide corresponding to residues 288–316 of cMCU (plus the C-terminal L and E as in the cMCU–ΔNTD construct) by chemical crosslinking using DTSSP (3,3′-dithiobis (sulfosuccinimidyl propionate)) (Thermo Scientific). Approximately 0.4 mg synthesized peptide (Pepmic Co., Ltd) was dissolved in 1 ml of reaction buffer (25 mM sodium phosphate, pH 7.5, and 50 mM NaCl) to a concentration of 0.1 mM. A stock solution of 30 mM DTSSP in water was prepared for addition to the peptide solution. Four samples, each containing 0.1 mM peptide in 30 μl reaction buffer were incubated with 0, 1, 3 and 5 mM DTSSP at room temperature. After 1 h, the reactions were quenched by adding 1 μl of stop solution (1 M Tris, pH 7.5). The reaction mixtures were analysed using SDS–PAGE. The SDS–PAGE results show that at DTSSP concentrations of 3 and 5 mM, the peptides could be crosslinked up to pentamers (Extended Data Fig. 7), indicating that the synthesized peptide can form pentamers in water.

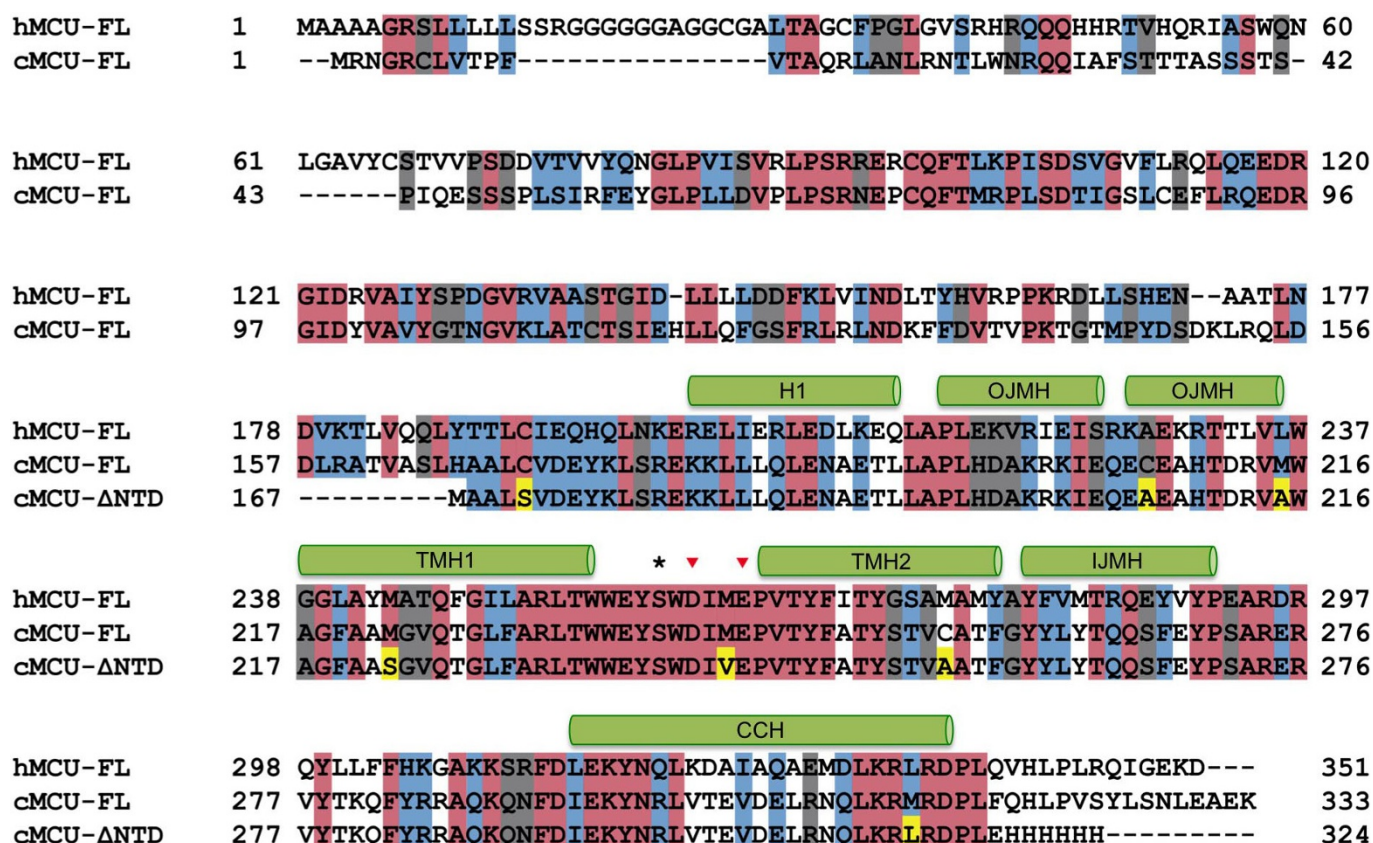**Functional mutagenesis of HsMCU.** *Material.* Reagents were obtained from the following sources: anti-Flag M2 affinity gel from Sigma (A2220), ATP5A antibody from Abcam (ab14748), Oregon Green 488 BAPTA-6 F from Life Technologies (O23990).

Cell culture and cell lines. MCU knockout cell lines were generated as previously described[7]. Cells were infected with lentivirus for stable expression of Flag-tagged proteins and selected with 100 μg ml^{-1} puromycin. Cell lines have been tested for mycoplasma contamination on a monthly basis using MycoAlert Mycoplasma Detection Kit (Lonza, LT07-418) and are free of mycoplasma contamination. The parental HEK-293T cell line has the following STR profile: TH01 (7, 9.3); D21S11 (28, 29, 30.2); D5S818 (7,8,9); D13S317 (11,12,13,14,15); D7S820 (11); D16S539 (9, 13); CSF1PO (11,12,13); Amelogenin (X); vWA (16,18,19,20); TPOX (11). This profile matches 100% to HEK-293T cell line profile (ATCC, CRL-3216) if the Alternative Master's algorithm is used, and 83% if the Tanabe algorithm is used. MCU knockout cell line was generated from this parental cell line by single cell cloning after MCU was knocked out using TALEN technology.

Calcium uptake in permeabilized HEK-293T cells. Calcium uptake assay in permeabilized HEK-293T cells was done as previously described[7]. Rate of calcium uptake is defined as the slope of the linear portion of the calcium uptake curve (between 20 and 30 s). In each experiment, calcium uptake rates of samples were normalized to the calcium uptake rate of a randomly selected wild-type HEK-293T cell uptake rate.

HsMCU-ΔNTD cloning and expression. For expression and mitochondrial targeting of HsMCU-ΔNTD, cDNA that corresponds to HsMCU amino acids 187–351 was fused to HsMCU mitochondrial targeting signal (amino acids 1–56) and cloned into pLYS1 vector as described previously[7].

28. Slotboom, D. J., Duurkens, R. H., Olieman, K. & Erkens, G. B. Static light scattering to characterize membrane proteins in detergent solution. *Methods* **46,** 73–82 (2008).
29. Tang, G. *et al.* EMAN2: an extensible image processing suite for electron microscopy. *J. Struct. Biol.* **157,** 38–46 (2007).
30. Ludtke, S. J., Baldwin, P. R. & Chiu, W. EMAN: semiautomated software for high-resolution single-particle reconstructions. *J. Struct. Biol.* **128,** 82–97 (1999).
31. Guo, X. *et al.* Structural insight into autoinhibition and histone H3-induced activation of DNMT3A. *Nature* **517,** 640–644 (2015).
32. Cong, Y., Kovacs, J. A. & Wriggers, W. 2D fast rotational matching for image processing of biophysical data. *J. Struct. Biol.* **144,** 51–60 (2003).
33. Cong, Y. *et al.* Fast rotational matching of single-particle images. *J. Struct. Biol.* **152,** 104–112 (2005).
34. Delaglio, F. *et al.* NMRPipe: a multidimensional spectral processing system based on UNIX pipes. *J. Biomol. NMR* **6,** 277–293 (1995).
35. Vranken, W. F. *et al.* The CCPN data model for NMR spectroscopy: development of a software pipeline. *Proteins* **59,** 687–696 (2005).
36. Bartels, C., Xia, T. H., Billeter, M., Guntert, P. & Wuthrich, K. The program XEASY for computer-supported NMR spectral analysis of biological macromolecules. *J. Biomol. NMR* **6,** 1–10 (1995).
37. Kay, L. E., Ikura, M., Tschudin, R. & Bax, A. Three-dimensional triple resonance NMR spectroscopy of isotopically enriched proteins. *J. Magn. Reson.* **213,** 423–441 (1990).
38. Salzmann, M., Wider, G., Pervushin, K. & Wuthrich, K. Improved sensitivity and coherence selection for [15N,1H]-TROSY elements in triple resonance experiments. *J. Biomol. NMR* **15,** 181–184 (1999).
39. Szyperski, T., Neri, D., Leiting, B., Otting, G. & Wuthrich, K. Support of ^{1}H NMR assignments in proteins by biosynthetically directed fractional ^{13}C-labeling. *J. Biomol. NMR* **2,** 323–334 (1992).
40. Schwieters, C. D., Kuszewski, J., Tjandra, N. & Clore, G. M. The Xplor-NIH NMR molecular structure determination package. *J. Magn. Reson.* **160,** 65–71 (2003).
41. Shen, Y., Delaglio, F., Cornilescu, G. & Bax, A. TALOS+: a hybrid method for predicting protein backbone torsion angles from NMR chemical shifts. *J. Biomol. NMR* **44,** 213–223 (2009).
42. Laskowski, R. A., MacArthur, M. W., Moss, D. S. & Thornton, J. W. PROCHECK: a program to check the stereochemical quality of protein structures. *J. Appl. Crystallogr.* **26,** 283–291 (1993).

```
hMCU-FL     1   MAAAAGRSLLLLLLSSRGGGGGGGAGGCGALTAGCFPGLGVSRHRQQQHHRTVHQRIASWQN   60
cMCU-FL     1   --MRNGRCLVTPF---------------VTAQRLANLRNTLWNRQQIAFSTTTASSSTS-   42

hMCU-FL    61   LGAVYCSTVVPSDDVTVVYQNGLPVISVRLPSRRERCQFTLKPISDSVGVFLRQLQEEDR  120
cMCU-FL    43   ------PIQESSSPLSIRFEYGLPLLDVPLPSRNEPCQFTMRPLSDTIGSLCEFLRQEDR   96

hMCU-FL   121   GIDRVAIYSPDGVRVAASTGID-LLLLDDFKLVINDLTYHVRPPKRDLLSHEN--AATLN  177
cMCU-FL    97   GIDYVAVYGTNGVKLATCTSIEHLLQFGSFRLRLNDKFFDTVPKTGTMPYDSDKLRQLD   156
```

                                        H1   OJMH   OJMH
```
hMCU-FL   178   DVKTLVQQLYTTLCIEQHQLNKERELIERLEDLKEQLAPLEKVRIEISRKAEKRTTLVLW  237
cMCU-FL   157   DLRATVASLHAALCVDEYKLSREKKLLLQLENAETLLAPLHDAKRKIEQCEAHTDRVMW   216
cMCU-ΔNTD 167   ---------MAALSVDEYKLSREKKLLLQLENAETLLAPLHDAKRKIEQEAEAHTDRVAW  216
```

                         TMH1   * ▼   ▼   TMH2   IJMH
```
hMCU-FL   238   GGLAYMATQFGILARLTWWEYSWDIMEPVTYFITYGSAMAMYAYFVMTRQEYVYPEARDR  297
cMCU-FL   217   AGFAAMGVQTGLFARLTWWEYSWDIMEPVTYFATYSTVCATFGYYLYTQQSFEYPSARER  276
cMCU-ΔNTD 217   AGFAASGVQTGLFARLTWWEYSWDIVEPVTYFATYSTVAATFGYYLYTQQSFEYPSARER  276
```

                                      CCH
```
hMCU-FL   298   QYLLFFHKGAKKSRFDLEKYNQLKDAIAQAEMDLKRLRDPLQVHLPLRQIGEKD---    351
cMCU-FL   277   VYTKQFYRRAQKQNFDIEKYNRLVTEVDELRNQLKRMRDPLFQHLPVSYLSNLEAEK   333
cMCU-ΔNTD 277   VYTKQFYRRAQKQNFDIEKYNRLVTEVDELRNQLKRLRDPLEHHHHHH--------   324
```

Extended Data Figure 1 | Multiple sequence alignment of the full-length hMCU, full-length cMCU and cMCU-ΔNTD. Residues that are invariant in all three sequences are shaded in red. Partially conserved and much less conserved residues are shaded in blue and grey, respectively. The mutations introduced in cMCU-ΔNTD are shaded in yellow. D and E in the DXXE motif are indicated by downward arrow. The serine residue shown to be involved in Ru360 inhibition is indicated by an asterisk[4]. Helical segments, as determined by NMR in this study, are indicated by cylinders and labelled as in the main text. The accession numbers for hMCU and cMCU are NM_138357.1 and NP_500892.1, respectively.
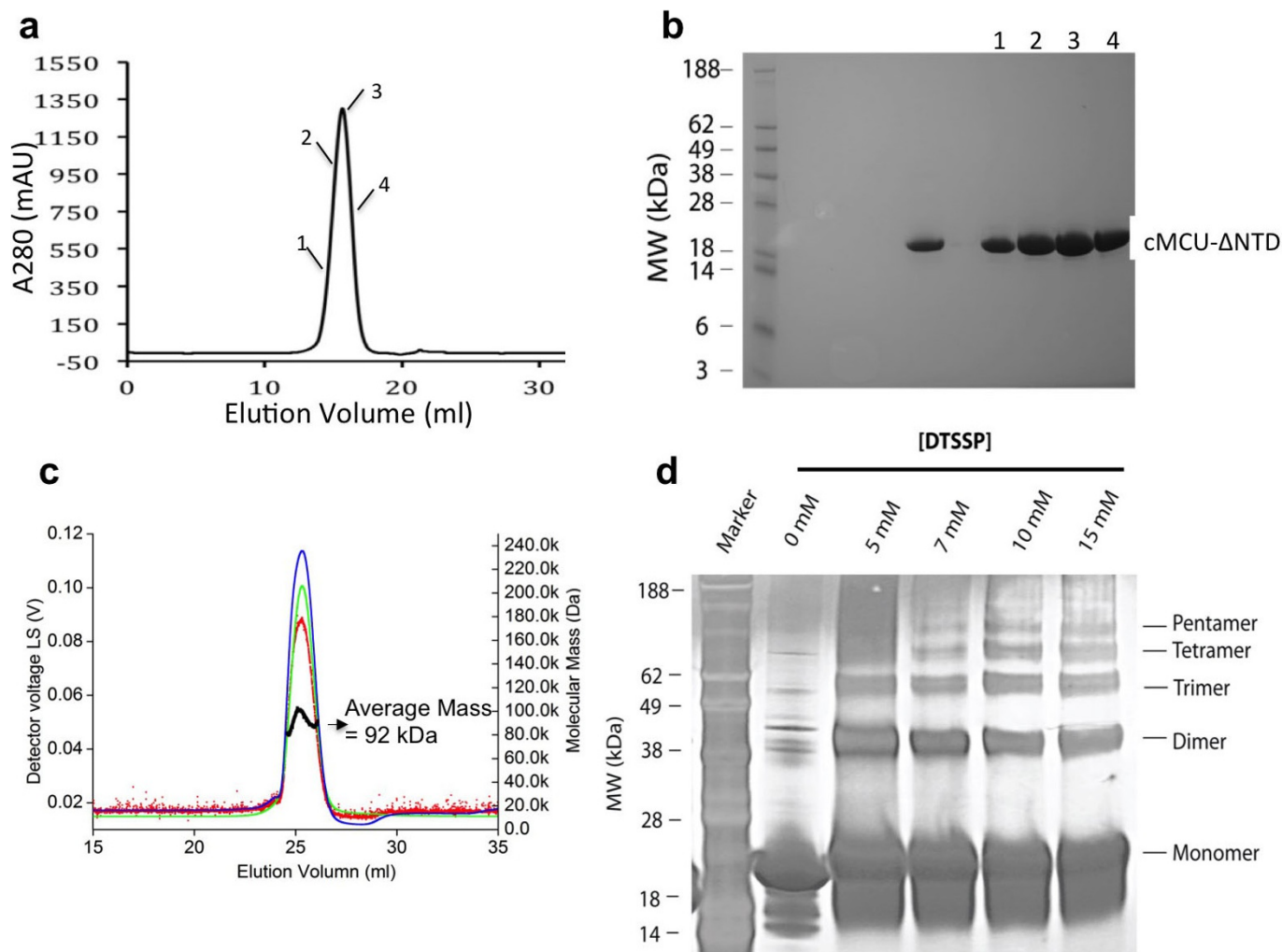
Extended Data Figure 2 | Biochemical analysis of cMCU-ΔNTD oligomeric state. a, Elution peak of cMCU-ΔNTD from Superdex 200 10/300 GL column in 20 mM MES, pH 6.4, 75 mM NaCl, 0.48 mM foscholine-14, 0.3 mM NaN_3 and 2 mM EDTA. **b**, SDS–PAGE analysis of the elution peak showing sample purity >95%. **c**, SEC-MALS analysis of the diluted NMR sample of cMCU-ΔNTD. The SEC-MALS/UV/ refractive index measurement was used to determine cMCU-ΔNTD molecular mass based on the three-detector method[28]. In this method, since the foscholine-14 detergent does not have UV absorption at 280 nm, the protein mass is directly calculated without correcting for the bound micelle. Chromatograms show the readings from the light scattering at 90° (red), refractive index (blue), and UV (green) detectors. The left and right axes represent the light scattering detector reading and molecular mass, respectively. The black curve represents the calculated molecular mass,

and the average mass of the elution peak of cMCU-ΔNTD is 92 kDa. Note the ~10 ml difference in elution volumes between **a** and **c** is due to the volume of solution feeding from SEC to MALS. **d**, SDS–PAGE analysis of chemical crosslinking of the diluted cMCU-ΔNTD NMR sample. The reaction mixture contains 0.1 mM cMCU-ΔNTD (monomer), 3 mM foscholine-14, and various amounts of DTSSP. The reactions were quenched after 1 h by the addition of 2 μl of 1 M Tris, pH 7.5. The quenched samples were loaded to 12% Bis-Tris gel (Novex Life Technologies). The gel was silver stained using the standard protocol. The five lanes to the right of the molecular mass marker correspond to DTSSP concentrations of 0, 5, 7, 10 and 15 mM. The band that corresponds to a pentamer showed the most obvious increase in intensity as a function of [DTSSP].
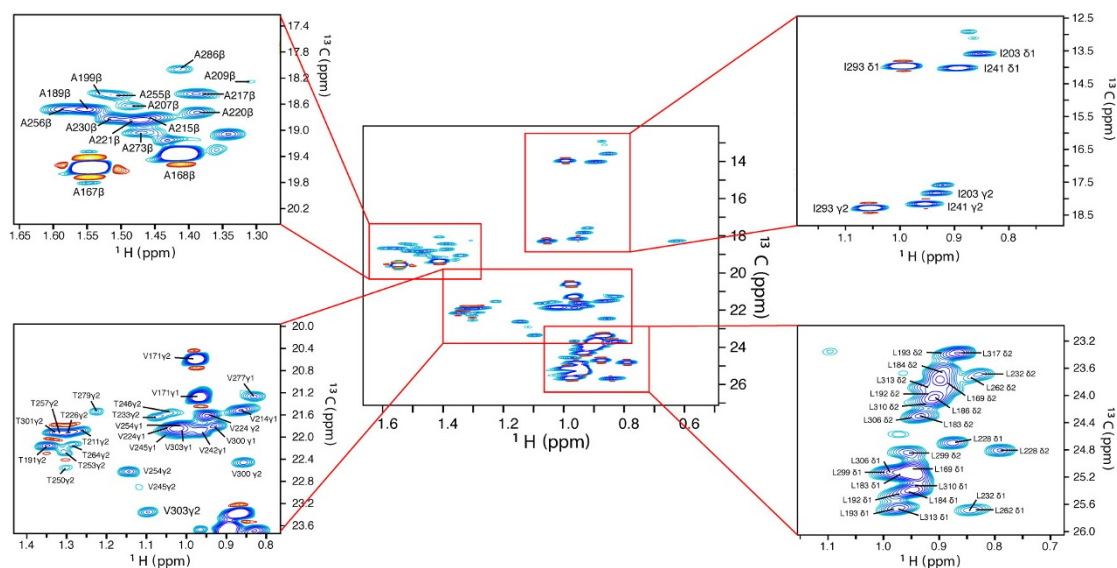
Extended Data Figure 3 | The cMCU-ΔNTD methyl group resonances with residue specific assignment. The ^{1}H–^{13}C HSQC was recorded with 28 ms constant-time ^{13}C evolution at 900 MHz.
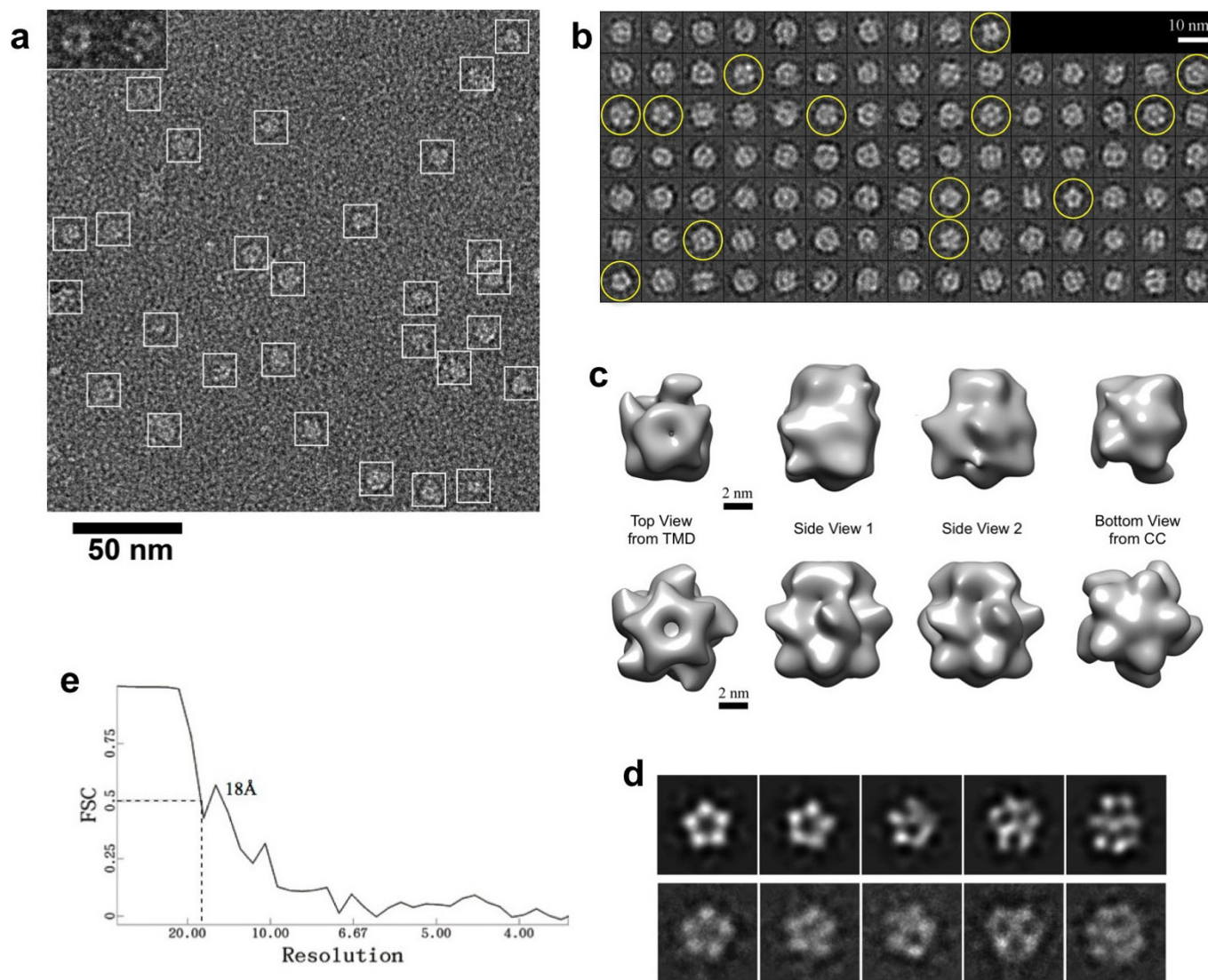
Extended Data Figure 4 | Single particle EM of the cMCU-ΔNTD oligomeric complex. a, Typical image of the cMCU-ΔNTD oligomers negatively stained with uranyl formate. The bar corresponds to 50 nm in length. A selected subset of cMCU-ΔNTD particles is highlighted with white circles. Shown in the top left corner are a typical top/bottom view and a typical side view of the selected particles. **b**, Gallery of 100 out of 202 reference-free 2D class averages of the particles, which revealed the existence of five-fold symmetry in the complex (pentagon shapes marked by yellow circles). **c**, Comparison of different views of the 3D EM density map reconstructed without enforcing C5 symmetry (top) with the corresponding views of the map reconstituted with symmetry (bottom). The largest discrepancies are in the middle bulge region between the TM and CC domains, possibly due to the lack of rigid structure in the large L2 loop. **d**, Comparison of the 2D projections (top) from the 3D EM density map with the corresponding reference-free 2D classes. **e**, Estimation of resolution of the final 3D reconstruction. The Fourier shell correlation (FSC) suggests a resolution of ~18 Å using the 0.5 criterion.
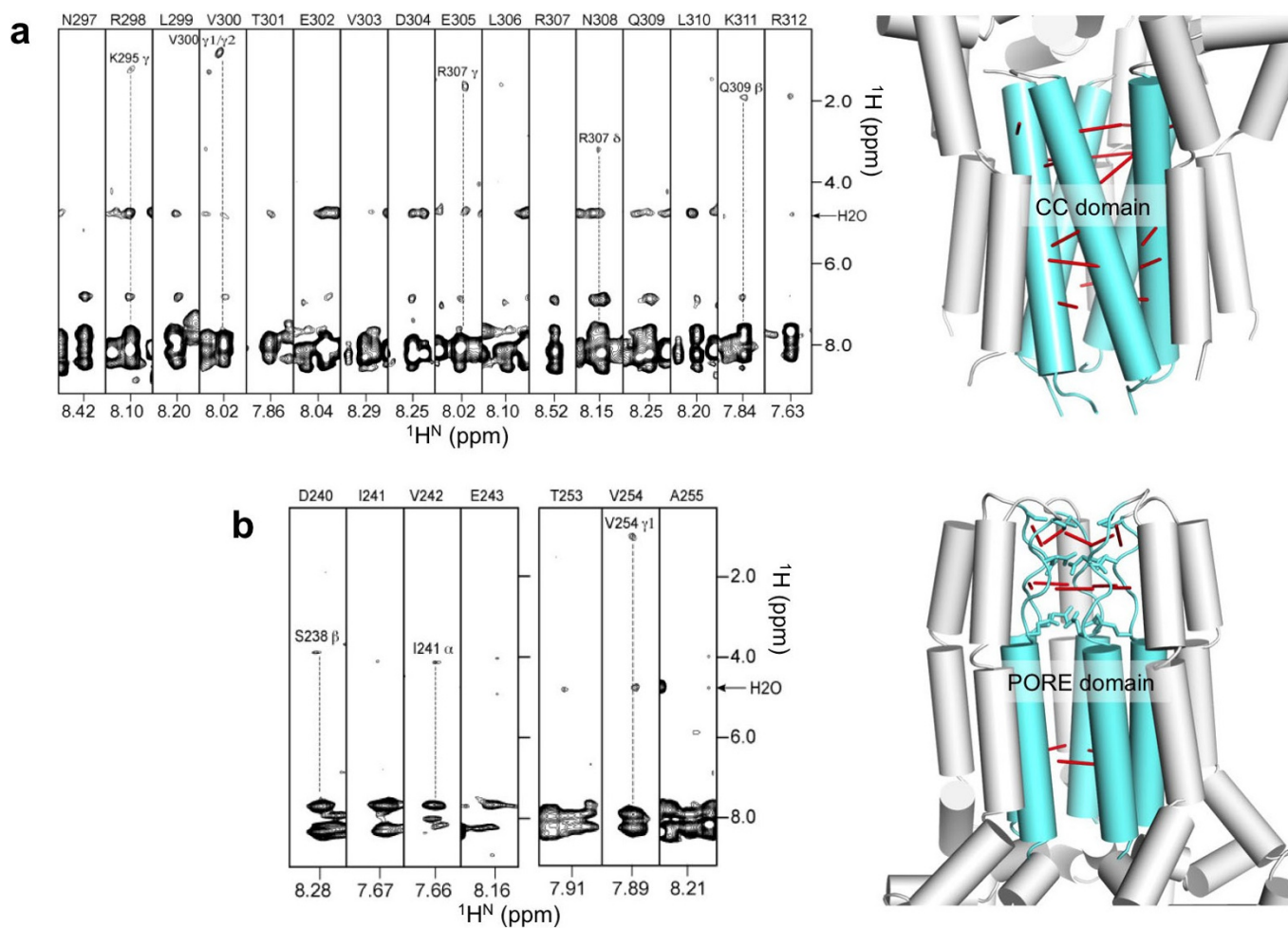
**Extended Data Figure 5 | Intermonomer NOEs from mixed isotope labelled sample.** Examples are taken from the 3D ^{15}N-edited NOESY-TROSY of the mixed labelled sample containing 1:1 mixture of (^{15}N, ^{2}H)-labelled cMCU-ΔNTD and (15% ^{13}C)-labelled cMCU-ΔNTD. **a**, Sample ^{1}H–^{1}H strips at various ^{15}N chemical shifts showing intermonomer NOEs between backbone amide proton and aliphatic protons for the C-terminal CCH domain. The NOE spectrum was recorded at 23 °C at 900 MHz. **b**, Sample strips showing intermonomer NOEs within the TMH2 pore as well as the selectivity filter region. The NOE spectrum was recorded at 33 °C at 900 MHz. On the right of each panel, intermonomer NOEs in the context of the structure are shown as red lines.
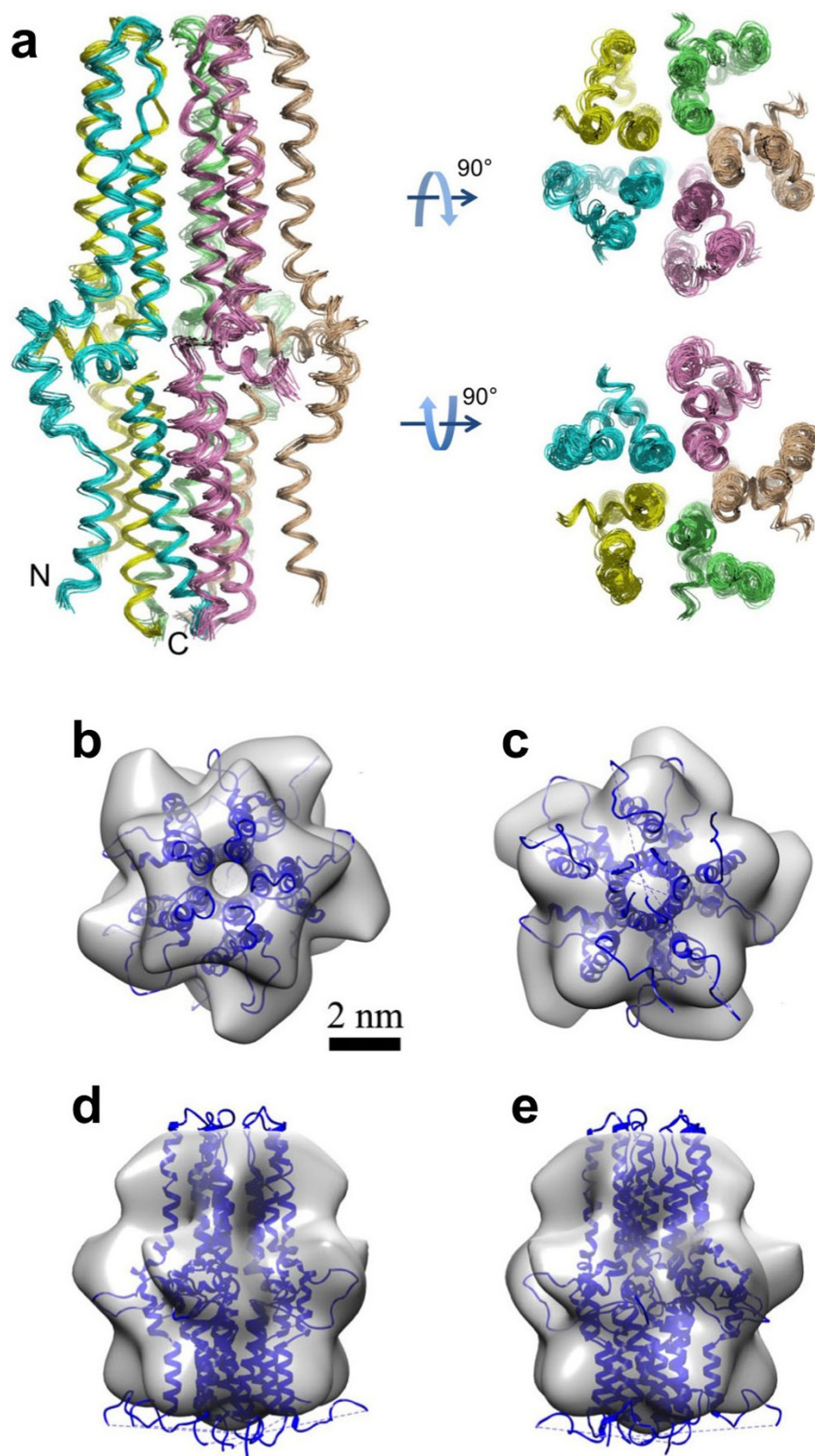
Extended Data Figure 6 | Structural ensemble of the cMCU-ΔNTD pentamer derived from NMR restraints and fitting to the EM density map. a, Ensemble of the 15 lowest-energy structures calculated using NMR-derived structural restraints (see Extended Data Table 1). The unstructured loops L1 (residues 166–179) and L2 (residues 272–292) are not shown for clarity. **b**, The NMR structure of cMCU-ΔNTD without the loop regions L1 and L2 was fitted to the EM volume using rigid body fitting (the 'fit' tool in Chimera). The L1 and L2 are however included for display. Top view from the intermembrane space side. **c**, Bottom view from the matrix side. **d, e**, Two different side views. Note that the loop regions appear disordered due to the lack of NMR-derived structural restraints. This does not necessarily mean that they do not acquire any stable conformation. The presumed detergent molecules around the membrane-embedded region are not taken into account in this fit.
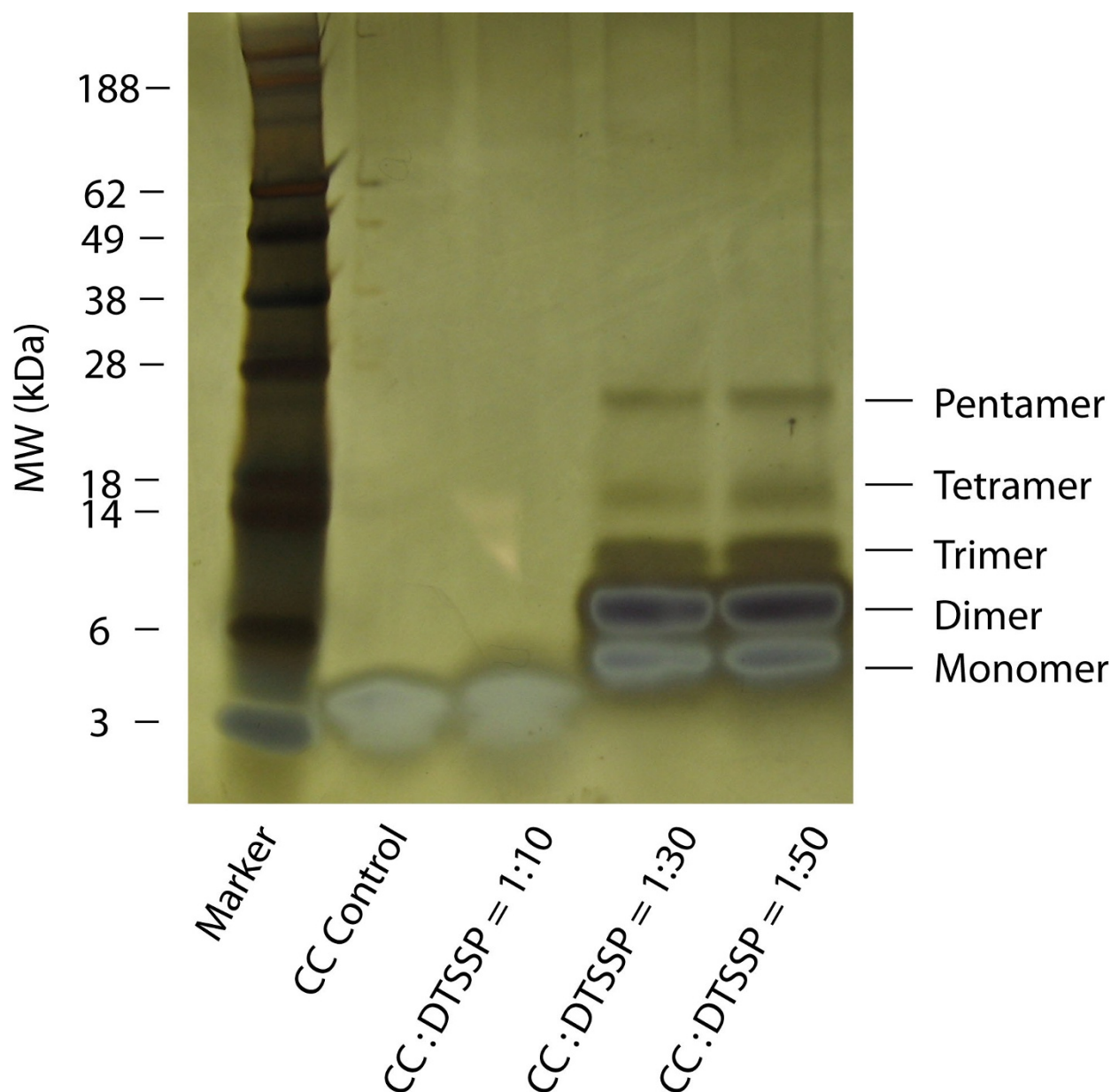
Extended Data Figure 7 | SDS–PAGE analysis of chemical crosslinking of the CCH peptide. The reaction mixtures containing 0.1 mM peptide (cMCU residues 288–316 plus the C-terminal L and E as in the cMCU-ΔNTD construct) and various amounts of DTSSP were quenched after 1 h of reaction by the addition of 1 μl of 1 M Tris, pH 7.5. The quenched samples were loaded to 12% Bis-Tris gel (Novex Life Technologies). The gel was silver stained using the standard protocol. The four lanes to the right of the molecular mass marker correspond to DTSSP:CCH ratios of 0, 10:1, 30:1 and 50:1.
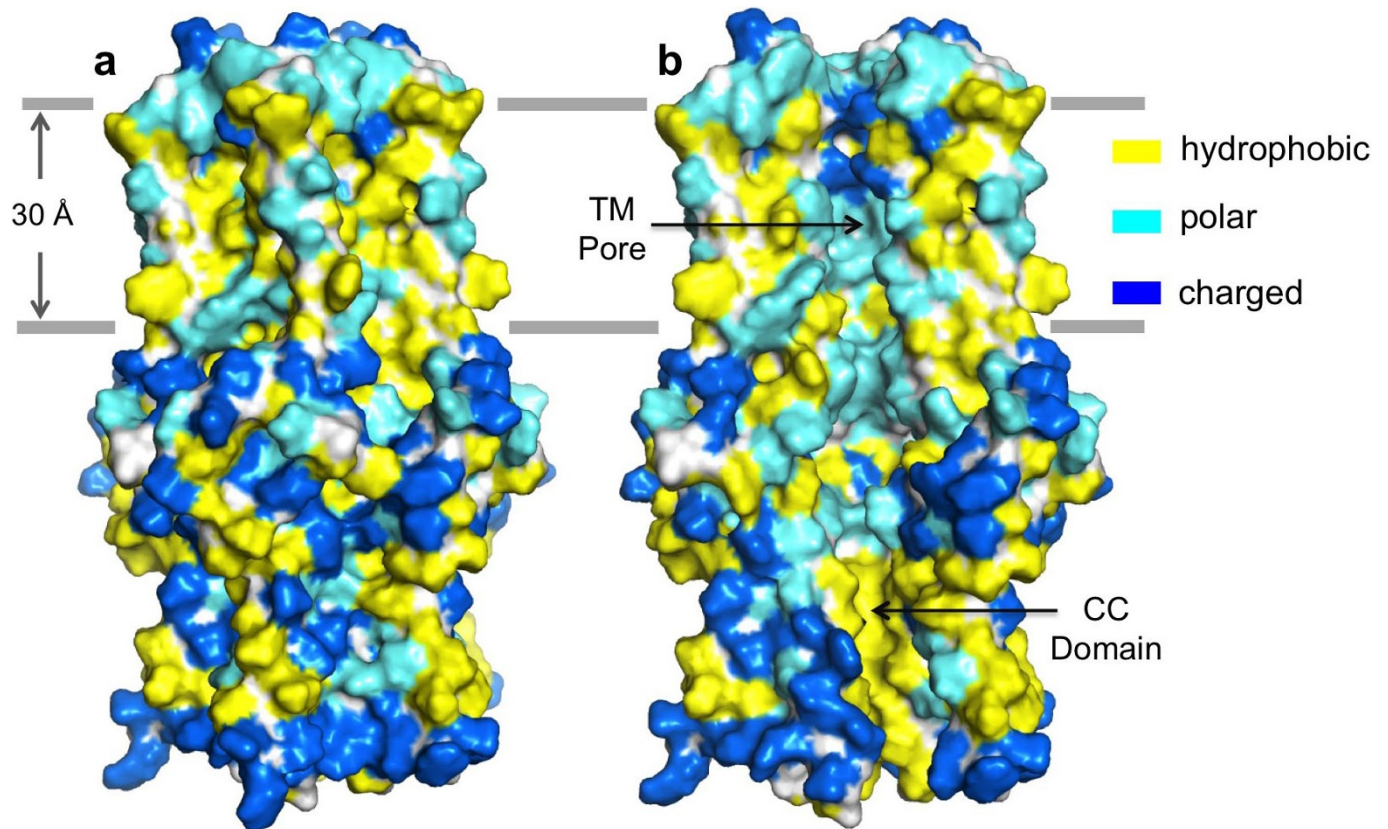
Extended Data Figure 8 | Surface representation for revealing the surface-exposed and core amino acid properties of the cMCU-ΔNTD pentamer. Hydrophobic, polar and charged residues are shown in yellow, cyan and blue, respectively. The hydrophobic residues include A, I, L, F, V, P and G, the polar residues include Q, N, H, S, T, Y, C, M and W, and the charged residues include K, R, D and E. The solid lines indicate the hydrophobic core boundaries of the presumed lipid bilayer. **a**, Pentamer with unstructured loops removed. **b**, The same view as in **a** but with the front subunit removed to reveal the core.
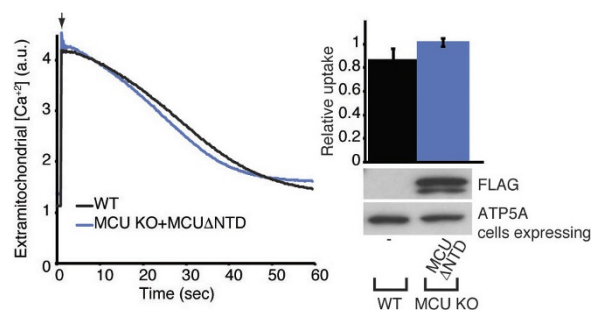
Extended Data Figure 9 | Deletion of the NTD (amino acids 58–186) in HsMCU (HsMCU-ΔNTD) does not impair its function. Representative traces of Ca^{2+} uptake in digitonin-permeabilized cells after addition of $50\,\mu M$ $CaCl_2$ are shown on the left. The bar graph shows the rate of Ca^{2+} uptake relative to wild-type HEK-293T cells (mean $\pm$ s.d., $n = 4$). Cell lysates were analysed by immunoblotting using an anti-Flag antibody to detect expression of MCU protein. ATP5A was used as loading control.

Extended Data Table 1 | NMR and refinement statistics for protein structures

	cMCU-ΔNTD
NMR distance and dihedral constraints	
Distance constraints	
Total NOE	2440
Intra-residue	130
Inter-residue	2310
Sequential ($|i\text{-}j| = 1$)	1280
Medium-range ($|i\text{-}j| < 4$)	660
Long-range ($|i\text{-}j > 5$)	150
Intermolecular	220
Hydrogen bonds	0
Total dihedral angle restraints	990
phi	495
psi	495
Structure statistics	
Violations (mean and s.d.)	
Distance constraints (Å)	0.231 ± 0.002
Dihedral angle constraints (°)	1.485 ± 0.034
Max. dihedral angle violation (°)	9.511
Max. distance constraint violation (Å)	1.487
Deviations from idealized geometry	
Bond lengths (Å)	0.034 ± 0.000
Bond angles (°)	1.777 ± 0.006
Impropers (°)	1.150 ± 0.016
Average pairwise r.m.s.d.** (Å)	
Heavy	1.503
Backbone	0.920

The numbers of constraints are summed over all five subunits. Backbone ϕ and ψ restraints of −60° and −40°, respectively, were assigned for regions of the protein confirmed to be helical based on local NOEs and TALOS+[39]. Statistics are calculated and averaged over an ensemble of the 15 lowest-energy structures out of 150 calculated structures. The precision of the atomic coordinates is defined as the average r.m.s.d. between the 15 final structures and their mean coordinates. The calculation includes only the structured regions of the protein: residues 180–192, 194–271 and 292–316.